

Current and vorticity auto correlation functions in open microwave billiards

Y.-H. KIM, M. BARTH, U. KUHL, and H.-J. STÖCKMANN *)

*Fachbereich Physik der Philipps-Universität Marburg, Renthof 5,
D-35032 Marburg, Germany*

Using the equivalence between the quantum-mechanical probability density in a quantum billiard and the Poynting vector in the corresponding microwave system, current distributions were studied in a quantum dot like cavity, as well as in a Robnik billiard with $\lambda = 0.4$, and an introduced ferrite cylinder. Spatial auto correlation functions for currents and vorticity were studied and compared with predictions from the random-superposition-of-plane-waves hypothesis. In addition different types of vortex neighbour spacing distributions were determined and compared with theory.

§1. Introduction

The large majority of wave functions of chaotic billiards is chaotic, i. e. at any point in the system, not too far from the wall, the wave function may be well described by a random-superposition of plane-waves (RSPW),¹⁾

$$\psi(\vec{r}) = \sum_n a_n \exp i\vec{k}_n \vec{r}, \quad (1)$$

where modulus $k = |\vec{k}_n|$ of the incoming wave is fixed, but directions \vec{k}_n/k and amplitudes are considered as random. As an immediate consequence the wave function amplitudes are Gaussian distributed, or, equivalently, their squares $\rho = |\psi|^2$ are Porter-Thomas distributed,

$$P(\rho) = \sqrt{\frac{A}{2\pi\rho}} \exp\left(-\frac{A}{2}\rho\right), \quad (2)$$

where A is the billiard area. For the spatial correlation function of the wave function amplitudes one obtains a Bessel function,

$$C(\vec{r}_1, \vec{r}_2) = \frac{\langle \psi^*(\vec{r}_1) \psi(\vec{r}_2) \rangle}{|\langle \psi(r) \rangle|^2} = J_0(kr), \quad (3)$$

where $r = |\vec{r}_1 - \vec{r}_2|$. The brackets denote an average over all positions. All these features have been demonstrated by McDonald and Kaufman in their influential work on stadium wave functions.^{2),3)} It is impossible to mention all papers which have been published hitherto on the subject. The RSPW approach is not restricted to quantum mechanics. This is why experiments using classical waves have played an important role, since for a long time they were the only ones with the ability to look

*) e-mails: young-hee.kim@physik.uni-marburg.de, michael.barth@physik.uni-marburg.de, ulrich.kuhl@physik.uni-marburg.de, stoeckmann@physik.uni-marburg.de

into the system. Very recently techniques have been developed which yield comparable information for electron flow patterns in mesoscopic structures.⁴⁾ The state of the art of the experiments with classical waves up to the year 1999 is presented in reference 5).

Most of the experiments with classical waves have been performed in microwave resonators^{6),7),8)} and vibrating solids.⁹⁾ In one work light propagation through a wave guide with distorted cross-section was studied.¹⁰⁾ In all cases the predictions of the RSPW approach could be verified. It should be noted that in the general case there is *no* one-to-one correspondence to quantum mechanics, thus demonstrating the universality of the approach. Therefore similar ideas have been developed independently in the context of room acoustics.¹¹⁾ Quasi-two-dimensional microwave resonators constitute one prominent exception where the equivalence to quantum mechanics is complete, including the boundary conditions. This is no longer true in three-dimensional resonators. But even here the approach remains valid.¹²⁾ One only has to superimpose plane *electromagnetic* waves with the consequence that expression (3) for the spatial autocorrelation function has to be modified.¹³⁾ Of course there are limitations. Since the RSPW approach completely ignores boundary conditions, deviations are expected and found in regions close to the boundary,^{14),15),16)} or if the wavelengths are not small compared to the system size.

The approach definitely cannot be applied to wave functions which are scarred along periodic orbits or show regular patterns associated with bouncing balls.¹⁷⁾ It was shown already by McDonald and Kaufman that for such wave functions the wave function amplitudes are *not* Gaussian distributed.³⁾ If the billiards are open, or if time-reversal symmetry is broken, the wave function are complex, and currents are present. In microwave experiments wall absorption is another source of currents. The quantum-mechanical probability density is given by

$$j(r) = \text{Im}(\psi^* \nabla \psi). \quad (4)$$

In quasi-two-dimensional electromagnetic cavities there is a one-to-one correspondence to the Poynting vector making an experimental determination of $j(r)$ feasible as well.¹⁸⁾

The consequences of the RSPW approach for the distribution of currents have been studied in particular by Berggren and coworker in a series of papers.^{19),20),21),22)} In open systems there are no longer nodal lines but nodal points, or vortices, since for the wave function to be zero both real and imaginary part have to be zero at the same time. Two-point correlation functions of vortices have been given independently by Berry and Dennis²³⁾ and by Saichev et al.²⁰⁾ Nearest neighbour distributions of vortices have been studied in Ref. 24). The theoretical predictions have been tested experimentally in two microwave experiments,^{25),26)} including a direct visualization of persistent currents well-known from mesoscopic physics. In the present paper a number of additional microwave tests of the RSPW hypothesis are presented with special emphasis on spatial auto correlation functions of currents and vorticities. To the best of our knowledge such quantities have never been studied before, neither theoretically nor experimentally. After a short recapitulation of the experimental

technique in section 2, analytic expressions for a number of autocorrelation function are derived in section 3. Various comparisons between experiment and theory are presented in section 4.

§2. Experiment

In the description of the experiment we can be short, since all details are available from our previous publications for the Robnik,^{25),26)} and the quantum dot billiard.²⁷⁾ The quantum dot billiard is an open billiard of rectangular shape with rounded corners, and an entrance and an exit wave guide attached at opposite sides (see Fig. 1). The second one belongs to the family of the Pascal limaçon, or Robnik billiards. It can be obtained by a complex mapping of the unit circle by means of the function $\omega = z + \lambda z$. For the parameter $\lambda = 0.4$, used in the experiment, the classical phase space is completely chaotic,²⁸⁾ apart from, perhaps, tiny regular fractions.²⁹⁾ A ferrite ring has originally been introduced to break time reversal symmetry thus giving rise to persistent currents. Time reversal symmetry is broken only for a small frequency region (approximately 3 to 5 GHz) but the absorption of the ferrite is present for the whole frequency range used for the data analysis (3 to 10 GHz). In the present context it is not of relevance whether the origin of the currents is break of time-reversal symmetry or absorption.

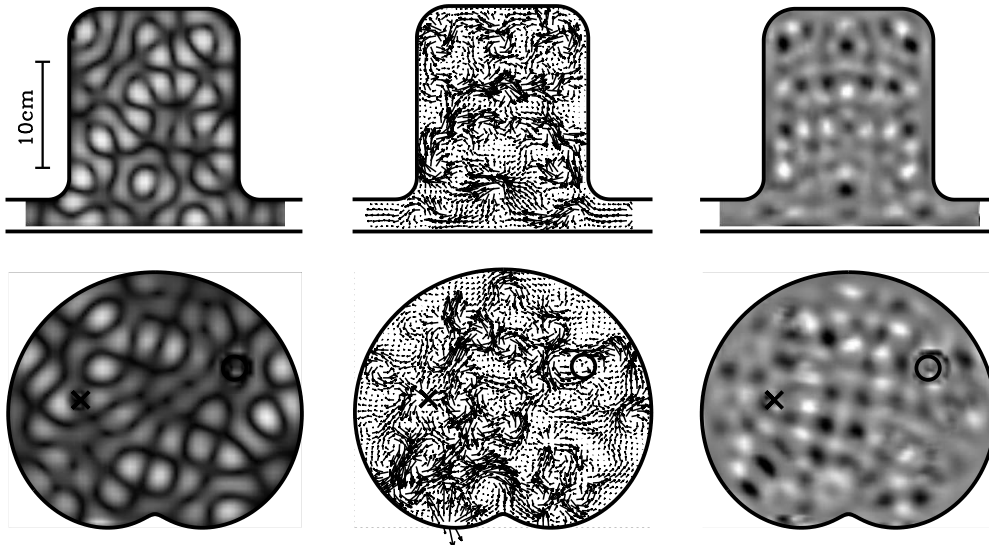


Fig. 1. Plot of wave function amplitude square $|\Psi|^2$, probability density $\vec{j} = \text{Im}(\Psi^* \nabla \Psi)$, and vorticity $\omega = (\nabla_x \Psi_R)(\nabla_y \Psi_i) - (\nabla_y \Psi_R)(\nabla_x \Psi_i)$ for the quantum dot billiard (upper row) at $\nu = 8.33$ GHz, and the Robnik billiard with a ferrite ring insert (lower row) at $\nu = 7.03$ GHz. The position of the antenna is indicated by a cross (\times). In the $|\Psi|^2$ plot (left column) the intensity is converted into a gray scale, where black corresponds to zero intensity. In the vorticity plot (right column) black corresponds to a large positive, and white to a large negative sense of rotation.

The linear dimensions of both cavities is of the order of 25 cm (see the scale in

Fig. 1), and their height is $h=8$ mm. For frequencies below 18.75 GHz there is a complete equivalence between the quantum mechanical wave function amplitudes ψ and the electric field E_z , where the quantum-mechanical eigenenergy E corresponds to the square of the wavenumber k^2 . Measuring the reflection amplitude at one antenna, or the transmission amplitude between two antennas, the complete scattering matrix can be obtained, which for isolated resonances reduces to a billiard Breit-Wigner function³⁰⁾

$$S_{ij} = \delta_{ij} - 2i\gamma \sum_n \frac{\text{Im}[\psi_n^*(r_i)\psi_n(r_j)]}{k^2 - k_n^2} \quad (5)$$

Both eigenfunctions and eigenenergies are slightly modified by the presence of the antenna which has been neglected in Eq. (5) (for an introductory presentation see chapter 6 of Ref. 5)). From a transmission measurement thus the wave function can be obtained including the sign, whereas a reflection measurement only yields the modulus.

For quasi-two-dimensional systems the Poynting vector $\vec{S} = c/(4\pi)\vec{E} \times \vec{H}$ reduces to¹⁸⁾

$$\vec{S} = \frac{c}{8\pi k} \text{Im}[E_z^*(r)\vec{\nabla}E_z(r)], \quad (6)$$

illustrating the one-to-one correspondence to the quantum mechanical probability density (4) stated above. Typical results for the two billiard systems under study are shown in Fig. 1. Further examples can be found in our previous publications.^{25),26)} In the right column $|\psi|^2$ is plotted in a gray scale for a typical frequency. The middle column shows the corresponding flow pattern as obtained from Eq. (6), where the arrows reflect the Poynting vectors at the respective points. The right column shows a plot of the vorticities, or vortex strengths. The vorticity is, up to the factor 1/2, just the curl of the current²³⁾ and reduces for two-dimensional systems to

$$\omega = (\nabla_x \psi_R)(\nabla_y \psi_I) - (\nabla_y \psi_R)(\nabla_x \psi_I), \quad (7)$$

where ψ_R, ψ_I are real and imaginary part of the wave function. A plot of the vorticity is particularly useful to make the vortex pattern visible as is evident from Fig. 1.

§3. Theory

It follows immediately from the RSPW hypothesis, as a consequence of the central limit theorem, that the $\psi(r)$ can be treated as Gaussian random variables. They obey the well-known property that all higher moments can be expressed in terms of the second moment. Thus all distributions of interest can be calculated.^{31),32)} We do not follow this route, however, mainly for pedagogical reasons, but start directly from Eq. (1) to calculate current and vorticity auto correlation functions.

Writing $\vec{k}_n = k(\cos \varphi_n, \sin \varphi_n)$, we obtain for the derivatives of the wave function

$$\begin{aligned}\frac{\partial\psi}{\partial x} &= ik \sum_n a_n \cos \varphi_n e^{i\vec{k}_n \vec{r}} \\ \frac{\partial\psi}{\partial y} &= ik \sum_n a_n \sin \varphi_n e^{i\vec{k}_n \vec{r}}\end{aligned}\quad (8)$$

Using Eq. (4), it follows for the x component of the current

$$j_x(\vec{r}) = k \sum_{n,m} a_n^* a_m (\cos \varphi_n + \cos \varphi_m) e^{-i(\vec{k}_n - \vec{k}_m) \vec{r}}. \quad (9)$$

In calculating the autocorrelation functions

$$C_{j_x}(\vec{r}_1, \vec{r}_2) \sim \langle j_x(\vec{r}_1) j_x(\vec{r}_2) \rangle \quad (10)$$

we use the assumption that the a_n are uncorrelated

$$\langle a_n^* a_m \rangle = \langle |a_n|^2 \rangle \delta_{nm}. \quad (11)$$

It follows from Eqs. (9) and (10)

$$\begin{aligned}C_{j_x}(\vec{r}_1, \vec{r}_2) &\sim k^2 \left\langle \sum_{n,m} |a_n|^2 |a_m|^2 (\cos \varphi_n + \cos \varphi_m)^2 e^{-i(\vec{k}_n - \vec{k}_m)(\vec{r}_1 - \vec{r}_2)} \right\rangle \\ &\sim \left\langle \cos^2 \varphi_n e^{-i\vec{k}_n \vec{r}} \right\rangle \left\langle e^{i\vec{k}_n \vec{r}} \right\rangle + \left\langle \cos \varphi_n e^{-i\vec{k}_n \vec{r}} \right\rangle \left\langle \cos \varphi_n e^{i\vec{k}_n \vec{r}} \right\rangle,\end{aligned}\quad (12)$$

where $\vec{r} = \vec{r}_1 - \vec{r}_2$. All averages can be expressed in terms of Bessel functions with the result

$$C_{j_x}(r) = \langle J_0(kr)[J_0(kr) - \cos 2\varphi J_2(kr)] + 2 \cos^2 \varphi [J_1(kr)]^2 \rangle, \quad (13)$$

where we have written $C_{j_x}(r)$ instead of $C_{j_x}(\vec{r}_1, \vec{r}_2)$ to indicate that the autocorrelation function depends on $r = |\vec{r}_1 - \vec{r}_2|$ exclusively. The normalization $C_{j_x}(0) = 1$ was applied. It only remains to perform the average over φ , the angle between vector \vec{r} and the x axis. The averaging gives

$$C_{j_x}(r) = [J_0(kr)]^2 + [J_1(kr)]^2. \quad (14)$$

For the autocorrelation function of $j_y(r)$ the same expression is obtained. Instead of averaging over φ , we may alternatively look for two other quantities, namely the autocorrelation functions of $j_{\parallel}(r)$, and $j_{\perp}(r)$, the current components parallel and perpendicular to \vec{r} , respectively. Inserting $\varphi = 0$ and $\varphi = \frac{\pi}{2}$ we obtain from Eq. (13)

$$\begin{aligned}C_{j_{\parallel}}(r) &= J_0(kr)[J_0(kr) - J_2(kr)] + 2J_1(kr) \\ C_{j_{\perp}}(r) &= J_0(kr)[J_0(kr) + J_2(kr)]\end{aligned}\quad (15)$$

In the same way the spatial autocorrelation function for the vorticity is obtained, entering definition (7) with expressions (8) for the derivatives of the wave function. The derivation is a step-by-step repetition of the calculation for $C_{j_x}(r)$, and we find

$$\begin{aligned} C_\omega(\vec{r}) &= \frac{\langle \omega(\vec{r}_1)\omega(\vec{r}_2) \rangle}{\langle \omega(\vec{r}_1)^2 \rangle} \\ &= [J_0(kr)]^2 - [J_1(kr)]^2 \end{aligned} \quad (16)$$

§4. Results

It was explained in Ref. 24) that there is a problem with the experimental determination of field and current distributions: the probe antenna moving through the billiard gives rise to a leakage current, which is critical close to positions where the field amplitudes are large. For the quantum dot billiard in addition there are frequencies where the total transmission is zero. In such a case the situation is even worse, since now there is exclusively the leakage current from the entrance to the probe antenna. All these problematic frequency regions have been omitted from the data analysis.

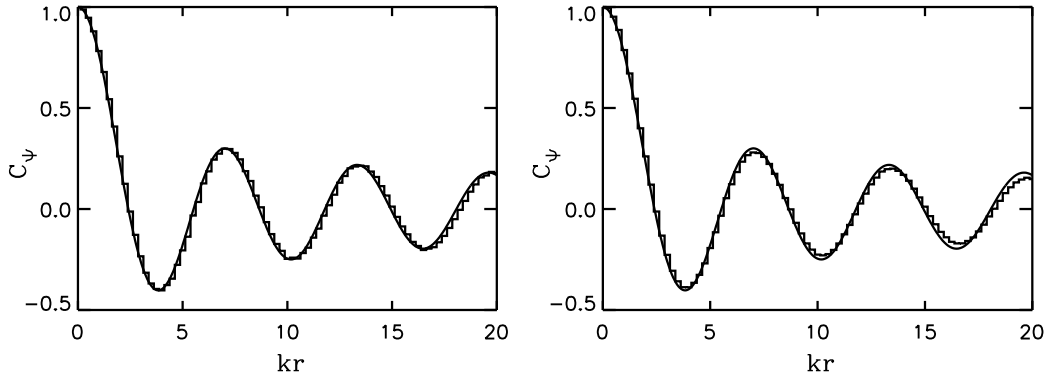


Fig. 2. Experimental spatial autocorrelation functions of the wave function amplitude for the quantum dot billiard (left) and the Robnik billiard with ferrite insert (right). The solid lines correspond to the prediction from the random-superposition of plane-waves approach (see Eq. (3)).

For the quantum dot billiard there is another problem. In the low-frequency regime the wave functions are still reminiscent of the rectangle with the checkerboard patterns typical for such systems. In addition there are frequencies showing strong scarring associated with bouncing balls and classical trajectories through the system. (The relation between scarring and transport was our original motivation to study this system,²⁷⁾ triggered by observations in correspondingly shaped quantum dots).

This is why for the quantum dot billiard only frequencies above 4.2 GHz were considered, where the system behaves chaotically. For both billiards at all frequencies used in the data analysis a Porter-Thomas distribution (2) of the squared wave function amplitudes is observed.

All correlation functions discussed in section 3 depend on the parameter kr ex-

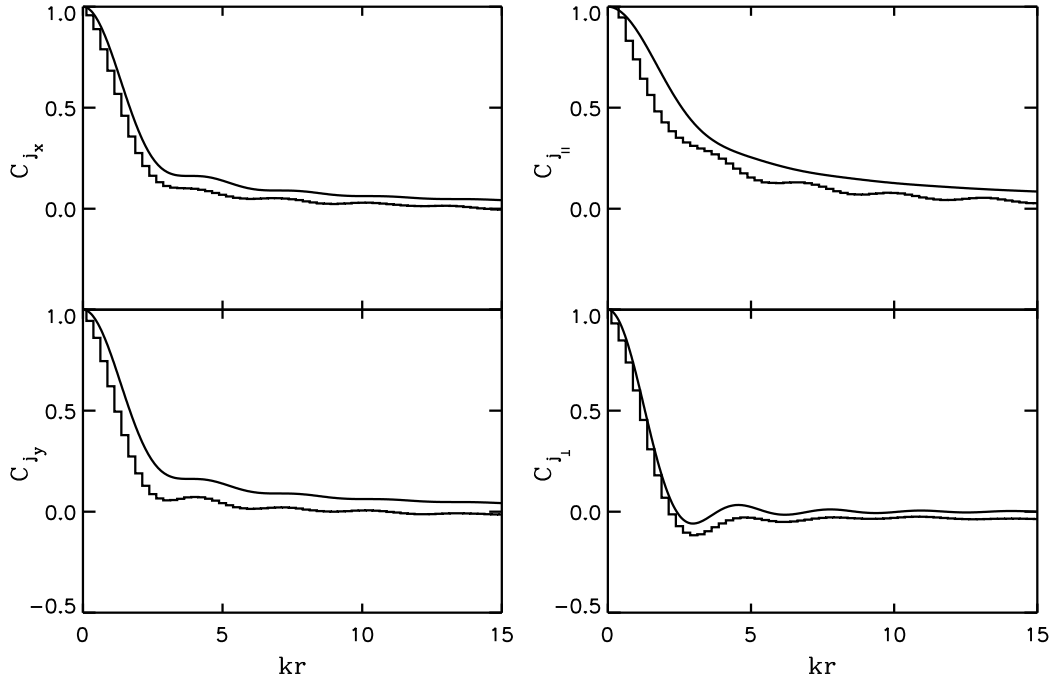


Fig. 3. Experimental spatial autocorrelation functions of $j_x(r)$, $j_y(r)$, $j_{\parallel}(r)$, and $j_{\perp}(r)$ (from top to bottom) for the quantum dot billiard (left column) and the Robnik billiard with ferrite insert (right column). The solid lines correspond to the predictions from the random-superposition of plane-waves approach (see Eqs. (14) to (15)).

clusively. Therefore it is possible to superimpose the results from different frequencies by an appropriate rescaling to improve statistics. We start with the presentation of our results for the spatial autocorrelation function of the wave function amplitudes (see Fig. 2). A perfect agreement is found for both systems between the experimental results and the prediction from the RSPW hypothesis. This may be considered as a check for the validity of the approach in the selected frequency regimes.

In Fig. 3, the results of the different current autocorrelation functions introduced in section 3, are shown for the Robnik billiard with ferrite insert. The corresponding figures for the quantum dot billiard have been omitted, since the results for the systems are more or less identical. Though there are deviations in detail, the overall qualitative agreement is very good. In particular the qualitatively different behaviour for the various types of current autocorrelation functions is reproduced correctly. For the vorticity autocorrelation function, shown in Fig. 4, the agreement between theory and experiment is nearly perfect. One only can speculate why this is the case: To determine the current, one needs the product of the wave function with its derivative, whereas the vorticity is obtained from the product of two derivatives. As a consequence, in the latter case all current offsets slowly varying with the position are eliminated. Therefore the vorticity is less sensitive on the mentioned experimental imperfections, as it seems.

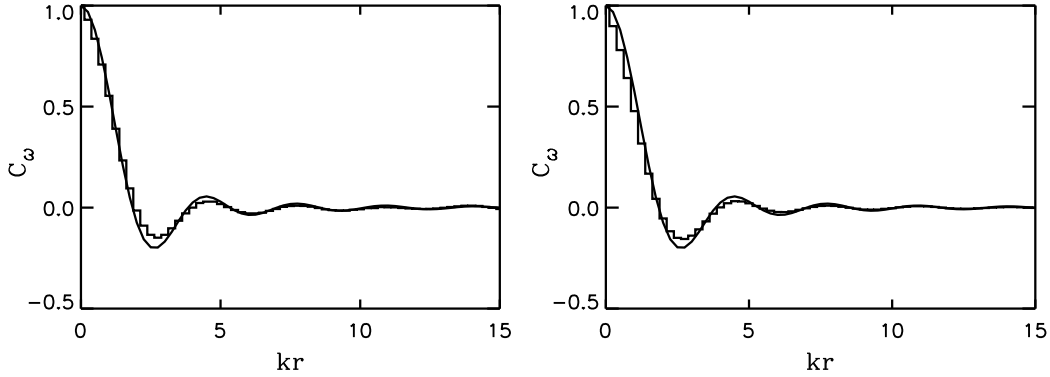


Fig. 4. Experimental spatial autocorrelation functions of the vorticity $\omega(r)$ for the quantum dot billiard (left) and the Robnik billiard with ferrite insert (right). The solid lines correspond to the predictions from the random-superposition of plane-waves approach (see Eq. (16)).

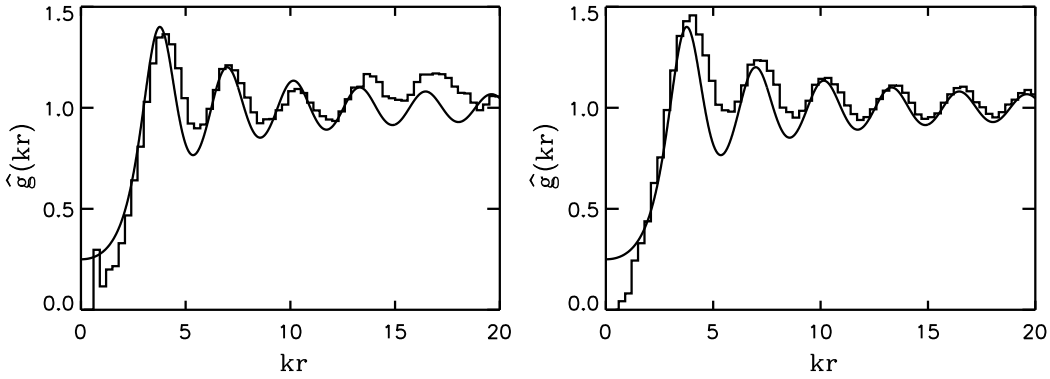


Fig. 5. Vortex pair correlation function for the quantum dot billiard (left) and the Robnik billiard with ferrite insert (right). The solid line corresponds to the theoretical prediction from the random-superposition-of-plane waves approach.^{23),20)}

In Fig. 5 vortex pair correlation functions for both systems are presented. Preliminary results for the Robnik billiard have already been shown in Ref. 24), where a more detailed discussion of this quantity can be found. The expected oscillatory behaviour again is reproduced correctly. The deviations between experiment and theory at small distances reflect the experimental resolution. The data were taken on a grid of 5 mm side length with the consequence that vortices with a distance below 10 mm can no longer be separated reliably.

We now extend this discussion to the nearest neighbour spacing distribution between vortices. This quantity was introduced by Saichev et al.²⁰⁾ and was studied by the authors in a number of papers. There are different types of spacing distributions denoted by $P_{++}(r), P_{+-}(r), P_{-+}(r), P_{--}(r)$ where the pair of indices denotes the sense of rotation of the vortices considered. $P_{++}(r)$ and $P_{--}(r)$, as well as $P_{+-}(r)$ and $P_{-+}(r)$ should be identical, of course. Only for small system sizes (where the RSPW approach fails anyway) there may be deviations due to the presence of the boundary.²⁰⁾ Fig. 6 shows our results, for $P_{++}(r)$ and $P_{+-}(r)$. Within the limits of

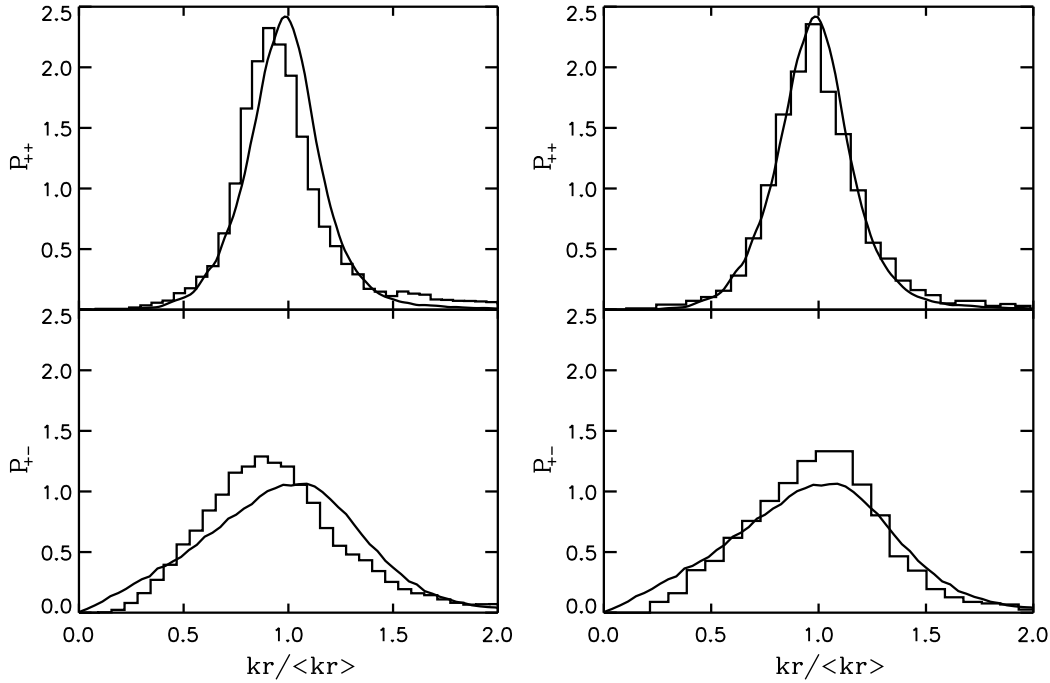


Fig. 6. Nearest neighbour distance distribution of vortices of opposite ($P_{+-}(r)$), and same sense of rotation ($P_{++}(r)$), respectively, for the quantum dot billiard (left), and the Robnik billiard with ferrite insert (right). The solid lines have been calculated from the respective pair correlation functions, neglecting higher order correlations.

statistical errors there was no difference to the corresponding distributions of $P_{--}(r)$ and $P_{-+}(r)$, respectively. The theoretical curve is the result of the Poisson approximation.²⁰⁾ It is obtained from the vortex pair-correlation functions and neglects all higher order correlations. The deviations between experiment and theory for $P_{+-}(r)$ are comparable to that found in the papers of the Berggren group,^{20),24)} and reflect at least partly the limitations of the Poisson approximation. Another cause, in particular for the small distances, is the limited experimental resolution discussed above. For $P_{++}(r)$, on the other hand, the agreement between experiment and theory is good, again in accordance with Refs. 20), 24). In addition, the experimental resolution has only a small effect in this case, since small distances do not contribute anyway to $P_{++}(r)$ significantly.

§5. Conclusion

In this paper a number of consequences of the RSPW hypothesis have been presented not been studied hitherto. A qualitatively good agreement between the experiment and the theoretical prediction was found for different types of spatial current correlation functions. The remaining discrepancies are probably due to experimental imperfections caused by leakage currents into the probe antennas. For

the vorticity autocorrelation function a perfect agreement between experiment and theory is found. In addition vortex pair correlation functions, and vortex nearest neighbour distance distributions were studied. Again the agreement between experiment and theory are good, apart from discrepancies at small distances.

Acknowledgements

The experiments were supported by the Deutsche Forschungsgemeinschaft. Rudi Schäfer, Marburg is thanked for helpful discussions. Part of the results presented in this paper were presented on the 5th International Summer school 2002 in Maribor. M. Robnik and his group is thanked for hospitality. The participation in the summer school was supported by the scientific and academic cooperation program between the universities of the twin towns Maribor and Marburg. K.-F. Berggren, Linköping is thanked for making his calculations of the vortex distance distributions available to us.

References

- 1) M.V. Berry, *J. Phys. A* **10**, 2083 (1977).
- 2) S.W. McDonald and A.N. Kaufman, *Phys. Rev. Lett.* **42**, 1189 (1979).
- 3) S.W. McDonald and A.N. Kaufman, *Phys. Rev. A* **37**, 3067 (1988).
- 4) M.A. Topinka *et al.*, *Science* **289**, 2323 (2000).
- 5) H.-J. Stöckmann, *Quantum Chaos - An Introduction* (University Press, Cambridge, 1999).
- 6) H.-J. Stöckmann and J. Stein, *Phys. Rev. Lett.* **64**, 2215 (1990).
- 7) S. Sridhar, *Phys. Rev. Lett.* **67**, 785 (1991).
- 8) H.-D. Gräf *et al.*, *Phys. Rev. Lett.* **69**, 1296 (1992).
- 9) C. Ellegaard *et al.*, *Phys. Rev. Lett.* **75**, 1546 (1995).
- 10) V. Doya, O. Legrand, F. Mortessagne, and C. Miniatura, *Phys. Rev. Lett.* **88**, 014102 (2002).
- 11) K.J. Ebeling, in *Statistical properties of random wave fields*, Vol. 17 of *Physical Acoustics: Principles and Methods*, edited by W.P. Mason and R.N. Thurston (Academic Press, New York, 1984), p. 233.
- 12) U. Dörr, H.-J. Stöckmann, M. Barth, and U. Kuhl, *Phys. Rev. Lett.* **80**, 1030 (1998).
- 13) B. Eckhardt, U. Dörr, U. Kuhl, and H.-J. Stöckmann, *Europhys. Lett.* **46**, 134 (1999).
- 14) A. Bäcker and R. Schubert, *J. Phys. A* **35**, 539 (2002).
- 15) M.V. Berry, *J. Phys. A* **35**, 3025 (2002).
- 16) A. Bäcker, S. Fürstberger, R. Schubert, and F. Steiner, Behaviour of boundary functions for quantum billiards, nlin.CD/0207034.
- 17) E.J. Heller, *Phys. Rev. Lett.* **53**, 1515 (1984).
- 18) P. Šeba, U. Kuhl, M. Barth, and H.-J. Stöckmann, *J. Phys. A* **32**, 8225 (1999).
- 19) K.-F. Berggren, K.N. Pichugin, A.F. Sadreev, and A. Starikov, *JETP Lett.* **70**, 403 (1999).
- 20) A.I. Saichev, K.-F. Berggren, and A.F. Sadreev, *Phys. Rev. E* **64**, 036222 (2001).
- 21) K.-F. Berggren, A.F. Sadreev, and A.A. Starikov, *Nanotechnology* **12**, 562 (2001).
- 22) A.I. Saichev, H. Ishio, A.F. Sadreev, and K.-F. Berggren, *J. Phys. A* **35**, L87 (2002).
- 23) M.V. Berry and M.R. Dennis, *Proc. R. Soc. Lond. A* **456**, 2059 (2000).
- 24) K.-F. Berggren, A.F. Sadreev, and A.A. Starikov, *Phys. Rev. E* **66**, 016218 (2002).
- 25) M. Barth and H.-J. Stöckmann, *Phys. Rev. E* **65**, 066208 (2002).
- 26) M. Vraničar *et al.*, *J. Phys. A* **35**, 4929 (2002).
- 27) Y.-H. Kim, M. Barth, H.-J. Stöckmann, and J.P. Bird, *Phys. Rev. B* **65**, 165317 (2002).
- 28) M. Robnik, *J. Phys. A* **16**, 3971 (1983).
- 29) H.R. Dullin and A. Bäcker, *Nonlinearity* **14**, 1673 (2001).
- 30) J. Stein, H.-J. Stöckmann, and U. Stoffregen, *Phys. Rev. Lett.* **75**, 53 (1995).
- 31) M. Srednicki, *Phys. Rev. E* **54**, 954 (1996).
- 32) M. Srednicki and F. Stiernelof, *J. Phys. A* **29**, 5817 (1996).